1-1-2020

Fe/Co-based Bimetallic MOF-derived Co3Fe7@NCNTFs Bifunctional Electrocatalyst for High-Efficiency Overall Water Splitting

Qunyao Yuan

Youxing Yu

Peter C. Sherrell
University of Wollongong, sherrell@uow.edu.au

Jun Chen
University of Wollongong, junc@uow.edu.au

Xiaofang Bi

Fe/Co-based Bimetallic MOF-derived Co3Fe7@NCNTFs Bifunctional Electrocatalyst for High-Efficiency Overall Water Splitting

Abstract

© 2020 Wiley-VCH Verlag GmbH & Co. KGaA, Weinheim Electrocatalytic water splitting to produce hydrogen and oxygen is regarded as one of the most promising methods to generate clean and sustainable energy for replacing fossil fuels. However, the design and development of an efficient bifunctional catalyst for simultaneous generation of hydrogen and oxygen remains extremely challenging yet is critical for the practical implementation of water electrolysis. Here, we report a facile method to fabricate novel N-doped carbon nanotube frameworks (NCNTFs) by the pyrolysis of a bimetallic metal organic framework (MIL-88-Fe/Co). The resultant electrocatalyst, Co3Fe7@NCNTFs, exhibits excellent oxygen evolution reaction (OER) activity, achieving 10 mA/cm2 at a low overpotential of just 264 mV in 1 M KOH solution, and 197 mV for the hydrogen evolution reaction. The high electrocatalytic activity arises from the synergistic effect between the chemistry of the Co3Fe7 and the NCNTs coupled to the novel framework structure. The remarkable electrocatalytic performance of our bifunctional electrocatalyst provides a promising pathway to high-performance overall water splitting and electrochemical energy devices.

Disciplines

Engineering | Physical Sciences and Mathematics

Publication Details

Yuan, Q., Yu, Y., Sherrell, P., Chen, J. & Bi, X. (2020). Fe/Co-based Bimetallic MOF-derived Co3Fe7@NCNTFs Bifunctional Electrocatalyst for High-Efficiency Overall Water Splitting. Chemistry - An Asian Journal, 15 (11), 1728-1735.

Fe/Co-based bimetallic MOF-derived Co_3Fe_7@NCNTFs bifunctional electrocatalyst for high-efficiency overall water splitting

Qunyao Yuan[1], Youxing Yu[1]*, Peter C. Sherrell[2,3], Jun Chen[3]*, and Xiaofang Bi[1]

[1]School of Materials Science and Engineering, Beihang University, Beijing 100191, China

[2]Department of Chemical Engineering, The University of Melbourne, Parkville, VIC 3010, Australia

[3]Intelligent Polymer Research Institute and ARC Centre of Excellence for Electromaterials Science, Australian Institute for Innovative Materials, University of Wollongong, Wollongong, NSW 2500, Australia

*Email: yuyouxing@buaa.edu.cn (Youxing Yu) and junc@uow.edu.au (Jun Chen)

ABSTRACT: Electrocatalytic water splitting to produce hydrogen and oxygen is regarded as one of the most promising methods to generate clean and sustainable energy for replacing fossil fuels. However, the design and development of an efficient bifunctional catalyst for simultaneous generation of hydrogen and oxygen remains extremely challenging, yet is critical for the practical implementation of water electrolysis. Here, we report a facile method to fabricate novel N-doped carbon nanotube frameworks (NCNTFs) by the pyrolysis of a bimetallic metal organic framework (MIL-88-Fe/Co). The resultant electrocatalyst, Co_3Fe_7@NCNTFs, exhibits excellent oxygen evolution reaction (OER) activity, achieving 10 mA/cm^2 at a low overpotential of just 264 mV in 1M KOH solution, and 197 mV for the hydrogen evolution reaction. The high electrocatalytic activity arises from the synergistic effect between the chemistry of the Co_3Fe_7 and the NCNTs coupled to the novel framework structure. The remarkable electrocatalytic performance of our bifunctional electrocatalyst provides a promising pathway to high-performance overall water splitting and electrochemical energy devices.

Keywords: MOF, Co_3Fe_7@NCNTFs, bifunctional electrocatalyst, overall water splitting

1. INTRODUCTION

The production of hydrogen from electrocatalytic water splitting through the hydrogen evolution reaction (HER) is an emerging technology to produce clean and sustainable fuels.[1] Typical water electrolysis process consists of two crucial half-reactions; the hydrogen evolution reaction (HER) and the oxygen evolution reaction (OER).[2] Therefore, it is critical to design and develop highly active and stable electrocatalysts for both HER and OER in order to improve the overall efficiency of a complete electrocatalytic water splitting cell.[3] Currently, platinum-based materials are the most efficient catalysts for HER while Ir/Ru-group compounds are the state-of-the-art catalysts for OER. [4] However, larger scale implementation of these noble metal-based electrocatalysts have been impeded by their scarcity, cost, and stability.[5] Thus, it is necessary to develop non-precious metal-based electrocatalysts with high efficiency and stability to promote electrocatalytic water splitting. In fact, many studies have attempted the development of these non-noble catalysts, using transition metals and their derivatives (i.e. transition metal oxides[6], carbides[7], sulfides[8] and phosphides[9]) or nanocarbon-based composites.[10] However, most of these materials suffer from poor stability and/or low conductivity.[11] One promising approach to enhance the electrocatalytic activity and durability of these non-noble catalysts is by embedding these nanoparticles into conductive porous carbon architectures.[12]

Metal organic frameworks (MOFs) consisting of metal moieties and organic linkers have been applied in various energy fields. For example, Dai et al, developed a novel MOF-derived material (Co@N-C) for Zn-air battery, which exhibits excellent performance (initial charge and discharge potential of 1.81 and 1.28 V under 2 mA cm^{-2}) and high cycling stability.[13] Sun et al, reported a novel metalorganic gaseous doping strategy to employ the typical ZIF-8 as template for preparing N-doped carbon polyhedron catalyst encapsulated with single Fe atoms for hydrogen-oxygen polymer electrolyte membrane fuel cell (PEMFC).[14] The resulting catalyst shows outstanding oxygen reduction reaction (ORR) activity and superb single-cell PEMFC performance. Recently, MOFs have been employed as templates for the synthesis of porous nanocarbon materials, due to their high porosity, large surface area and accessible active sites.[13, 15] However, most of these MOF-based nanocarbons have been found with a microporous structure and low degree of graphitization, which are unfavorable for mass transport and limit electrical conductivity.[16] A number of interesting works have been reported on using MOFs as precursors for the preparation of hybrids with metallic nanoparticles embedded carbon nanotubes (CNTs).[17] For instance, Lou *et al*. verified that using ZIF-67 as precursor for constructing CNT frameworks with encapsulated Cobalt nanoparticles resulted in excellent conductivity and stability,

benefiting from the formation of a robust hollow structure composed of CNTs. [5a] Thomas *et al*. employed a MOF precursor as the template to prepare with metal nanoparticles embedded CNT networks which exhibited enhanced electrocatalytic activity.[16] However, in these works, the as-obtained CNTs either exhibits poor electrocatalytic activity or do not retain any secondary microstructure.

In this work, we developed a strategy for the synthesis of non-noble metal based, MOF-derived, bifunctional electrocatalysts. This was achieved via the *in-situ* growth of N-doped carbon nanotube (NCNT) frameworks with embedded Co_3Fe_7 nanoparticles (denoted Co_3Fe_7@NCNTFs) through a one-pot carbonization of a bimetallic MIL-88-Fe/Co precursor. The as-synthesized Co_3Fe_7@NCNTFs perfectly retain the structure of the original framework (MIL-88-Fe/Co) with many interlaced NCNTs grown within the architectures. Benefiting from the merits of robust N-doped CNTs (NCNTs), the resulting Co_3Fe_7@NCNTFs electrocatalyst exhibits remarkable bifunctional catalytic activities, showing an overpotential of 264 mV (OER) and 197 mV (HER) to reach a current density of 10 mA/cm^2 in 1M KOH solution, respectively. Its superior water electrolysis performances outperform various reported nanocarbon materials so far, making it be a promising high-efficiency non-precious bifunctional catalyst for water splitting.

2. EXPERIMENTAL SECTION

2.1. Chemical and Materials. terephthalic acid (BDC), $Co(NO_3)_2{\cdot}6H_2O$ and $FeCl_3{\cdot}6H_2O$ were purchased from Macklin. Ethanol (C_2H_5OH), N,N-Dimethylformamide (DMF) and sodium hydroxide (NaOH) were obtained from Beijing Chemical Work. All chemical reagents were used without any further purification. Ultrapure water (resistance of 18.2 MΩ·cm at 25 °C) was used for all experiments.

2.2. Preparation of Electrocatalysts. *2.2.1. Synthesis of MIL-88-Fe/Co nanorods.* Briefly, a mixture of 0.66 mmol $FeCl_3{\cdot}6H_2O$, 0.33 mmol $Co(NO_3)_2{\cdot}6H_2O$ and 0.99 mmol terephthalic acid were dissolved in 10 mL N,N-dimethylformamide (DMF) with continuously stirring for 15 min to obtain a clear solution. Then, 2 mL 0.4 M NaOH solution was injected dropwise into the above mixture solution under stirring. After stirring for 30 min, the mixture solution was transferred to the 25 mL Teflon-lined stainless-steel autoclave and the autoclave was heated in an electric oven at 115 ℃ for 24 h, later naturally cooled down to the room temperature. Finally, the resulting brown product was centrifuged and watered with DMF and ethanol for 4 times and dried at 50 °C in vacuum for overnight.

2.2.2. Synthesis of Co_3Fe_7@NCNTFs Catalyst. The obtained MIL-88-Fe/Co was fully ground with equal quality dicyandiamide (DCDA) in a quartz mortar. The mixed powder was then placed in a ceramic

boat and heated to 600 °C at a heating rate of 2 °C/min and maintained this temperature for 3 hours in vacuum in the tube furnace.

2.2.3. Synthesis of Co_3Fe_7@C Catalyst. In order to show the role of DCDA for generating N-doped carbon nanotubes (NCNTs), the Co_3Fe_7@C was also obtained as a comparison which was obtained according to the same method as Co_3Fe_7@NCNTFs but without DCDA addition.

2.2.4. Synthesis of Co-Fe@NC-powder. As a comparison, the Co-Fe@NC-powder was prepared by mixing $FeCl_3 \cdot 6H_2O$, $Co(NO_3)_2 \cdot 6H_2O$, terephthalic acid (BDC) and DCDA (equal mass with as-prepared MIL-88-Fe/Co), and then grinded to obtain homogeneous solid. The resulting solid powder was transferred to the tube furnace at the same heat condition as Co_3Fe_7@NCNTFs.

2.3. Materials Characterizations. The X-ray diffraction (XRD) of MOF precursors and pyrolysis products were measured on Rigaku D/max 2500 with a Cu Kα radiation source (λ = 1.54056 Å) at a generator voltage of 40 kV and a generator current of 200 mA with a scanning speed of 5 °/min from 5° to 50° for MOF precursor (powder) and from 5° to 90° for samples (powder). Raman spectroscopy was conducted on Horiba Scientific-LabRAM HR Evolution with an excitation wavelength of 532 nm. A scanning electron microscope (ZEISS-SUPRA55) at an operating voltage of 10 kV and a transmission electron microscope (JEOL, JEM-2100) at an operating voltage of 200 kV were used to obtain the SEM and TEM images, respectively. X-ray photoelectron spectroscopy (XPS) was performed on a Thermo Scientific ESCALab 250Xi with 150 W monochromatic Al Kα radiation. The base pressure in the analysis chamber was approximately 1×10^{-10} mbar. The hydrocarbon C 1s line at 284.8 eV from adventitious carbon was used for binding energy referencing.

2.4. Electrochemical Measurements. All electrochemical measurements except the overall water splitting reaction were conducted in a standard three-electrode cell on a CHI650D electrochemical workstation at room temperature. The catalyst ink was obtained as a mixture of 5 mg catalyst powder, 750 μL ethanol, 200 μL DI water and 50 μL 5% Nafion solution. The as-synthesized powder catalysts were examined by coating the catalyst ink onto the glassy carbon electrode (diameter: 3.0 mm, area: 0.0706 cm^2) with a mass loading of 0.35 mg/cm^2 as the working electrode. Prior to measurement, the coated glassy carbon electrode/catalyst ink was allowed to air dry overnight. A Hg/HgO (1M KOH) electrode and graphite rod were used as the reference and counter electrode, respectively, with 1M KOH used as the electrolyte. The hydrogen evolution reactions (HER) and oxygen evolution reactions (OER) were performed via linear sweep voltammetry with a scan rate of 2 mV/s with 85% *iR*-correction. All

electrochemical potential values for the three-electrode configuration used in this study were changed from *E* (Hg/HgO) to *E* (RHE) via the following equation:

$$E\ (\mathrm{RHE}) = E\ (\mathrm{Hg/HgO}) + 0.098 + 0.05916 \times \mathrm{pH}$$

where $E_{Hg/HgO}$ was the measured potential against the reference electrode.[18]

Electrochemical impedance spectroscopy (EIS) was carried out at the overpotential at a current density of 10 mA/cm^2 (as determined by linear sweep voltammetry described above) with a frequency range from 0.01 Hz to 100 kHz. The stability test of Co_3Fe_7@NCNTFs was carried out with a i-t curve at the potential of current density at 10 mA/cm^2.

The overall water splitting performance was tested by employing a two-electrode configuration in 1 M KOH solution with a scan rate of 2 mV/s without any *iR*-compensation. The cathode and anode for overall water splitting were obtained by coating the catalyst ink onto 1×1 cm Ni foam and keeping the same mass loading of 0.35 mg/cm^2.

3. RESULTS AND DISCUSSION

3.1. Physicochemical Analysis. The typical two-step synthetic route of Co_3Fe_7@NCNTFs is schematically illustrated in **Figure 1a**. Firstly, the MIL-88-Fe/Co precursor was prepared by a solvothermal method at 115 ºC for 24 h (**Figure S1**). Then, the as-prepared MIL-88-Fe/Co powder was physically ground together with dicyandiamide (DCDA) powder (at 1:1 mass ratio) to form a uniform mixture. The obtained mixed powder was transferred to a quartz boat and pyrolyzed at 600 °C for 3 h under vacuum to synthesize the nitrogen-doped carbon nanotube frameworks (NCNTFs) with embedded Co_3Fe_7 nanoparticles (denoted Co_3Fe_7@NCNTFs). Field-emission scanning electron microscopy (FESEM) clearly demonstrates the phase transformation from the homogeneous rod-shaped MIL-88-Fe/Co precursor (**Figure 1b**) to the final as-obtained Co_3Fe_7@NCNTFs (**Figure 1c**) with the appearance of interlaced CNTs grown out of MOF rod structures.

Further investigation using transmission electron microscopy (TEM) was carried out to confirm the structure of the CNT networks protruding the rod-like morphology of pyrolyzed frameworks (**Figure 2a**), highlighting the intimate connections between the structures. In addition, the high-resolution TEM (HRTEM) also reveals that Co_3Fe_7 nanoalloys are embedded in the highly graphitized carbon shells of the carbon nanotubes, showing an interplanar distance of ~0.37 nm corresponding to (002) lattice plane of graphitic carbon (**Figure 2b**). The encapsulated nanoparticle has an interplanar distance of 0.200 nm (**Figure 2c, d**), which corresponds to the (110) lattice plane of Co_3Fe_7 nanoalloys. Such unique

architectures with nanoalloys embedded in the NCNT frameworks provides several clear potential advantages for electrocatalysis. The unique architectures could enhance the electrical conductivity and improve the charge transfer from the catalyst to the electrode, while also avoiding the aggregation of Co_3Fe_7 nanoparticles by the physical separation achieved by coverage with multi-graphitic layers.

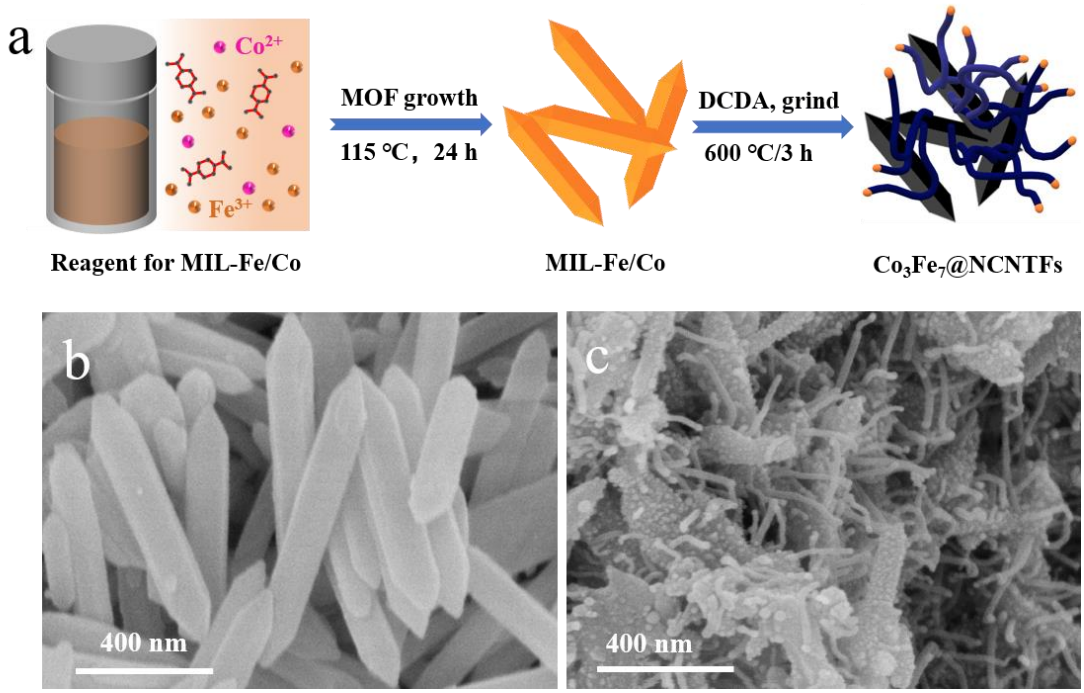

Figure 1. (a) Schematic illustration of two-step synthesis of Co_3Fe_7@NCNTFs; **(b** and **c)** high-resolution SEM images of as-prepared **(b)** MILF-88-Fe/Co and **(c)** Co_3Fe_7@NCNTFs.

The role of DCDA during the annealing step for the preparation of Co_3Fe_7@NCNTFs has been further investigated via the comparison with control sample of Co_3Fe_7@C, which was prepared by the direct pyrolysis of MIL-88-Fe/Co precursor without DCDA. No CNTs growth has been observed on the surface of the carbon framework in the absence of DCDA (**Figure S2**), further only partially reduced metal nanoparticles are embedded in the carbon framework for Co_3Fe_7@C (**Figure S3**). Previous studies have demonstrated that reduction atmosphere is essential for the formation of CNTs when MOFs are employed as precursors.[5a] In this work, it can be reasonably assumed that DCDA plays a critical role in not only introducing a N source but providing the reducing atmosphere required for the growth of N-doped CNTs. Typically, during the annealing process, DCDA was firstly decomposed into NH_3, which then was quickly reduced the surface metal ions of MIL-88-Fe/Co into metal nanoparticles. Then, these nanoparticles further catalyzed the NCNTs growth from the MOF surface to form the expected Co_3Fe_7@NCNTFs.[19] On the other hand, in order to study the effect of MOF precursor's crystal structure and morphology on final catalyst's electrocatalytic performance, a comparative experiment (which

avoided the use of the synthesized MIL-88-Fe/Co) used $Co(NO_3)_2 \cdot 6H_2O$, $FeCl_3 \cdot 6H_2O$, terephthalic acid, mixed with DCDA, were directly annealed under the identical pyrolysis conditions (denoted Co-Fe@NC-powder, for detailed information see **Figure S4**) as control.

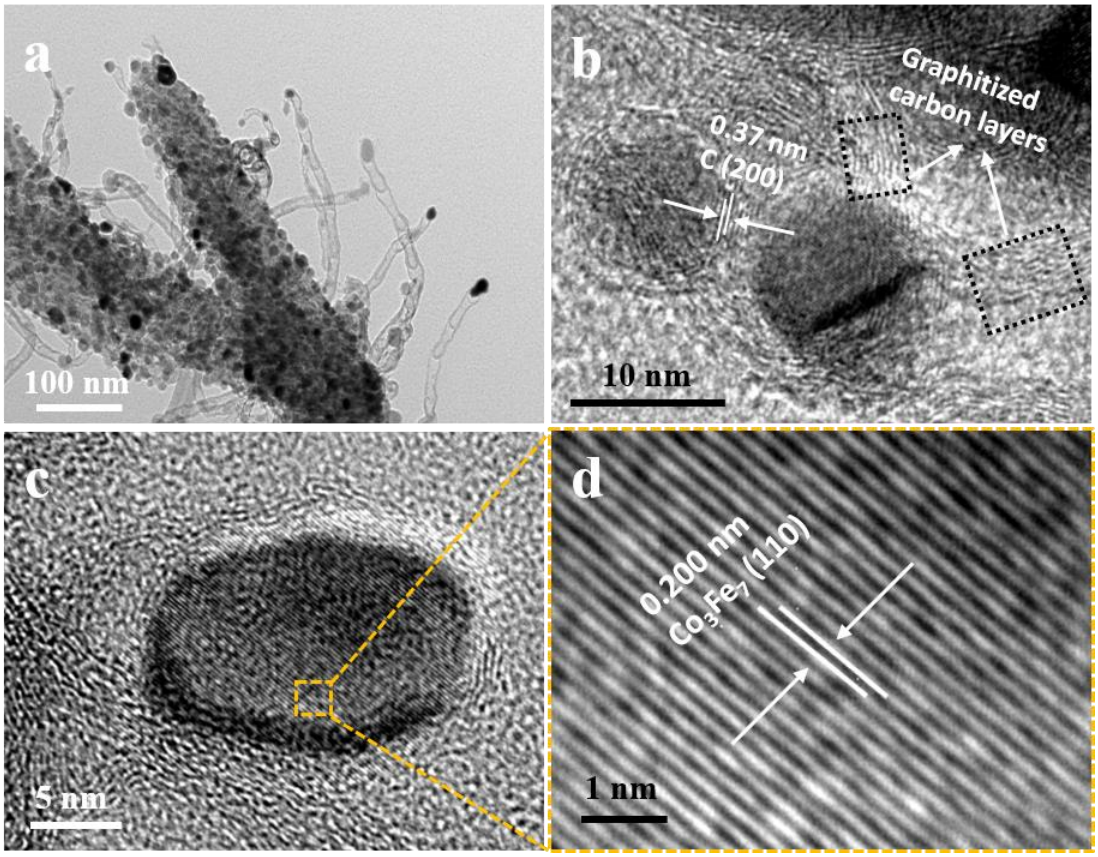

Figure 2. HRTEM images of **(a, b)** Co_3Fe_7@NCNTFs; and **(c, d)** the embedded of Co_3Fe_7 nanoalloy.

Powder X-ray diffraction (PXRD) measurements were conducted to identify the crystal structure and phases of the final electrocatalysts. As **Figure 3a** shows, Co_3Fe_7@NCNTFs shows a distinct graphitic carbon peak near 26° which is not sharp or clear in Co_3Fe_7@C, indicating the higher graphitic degree in Co_3Fe_7@NCNTFs. However, for the Co-Fe@NC-powder sample, this traditional graphitic carbon peak is not observed at all. In fact, this has been confirmed by the electron microscopy analyses, showing no carbon framework in the pyrolyzed Co-Fe@NC-powder (**Figure S4**). Furthermore, the peaks at 44.7°, 65.1° and 82.4° for all three samples are assigned to (110), (200) and (211) diffractions of Co_3Fe_7 alloy (JCPDS no. 48-1817),[20] which is consistent with the TEM results. In addition, there are additional peaks related to $CoFe_2O_4$ (JCPDS no.22-1086) observed in the Co-Fe@NC-powder sample. Raman spectroscopy was also used to probe the degree of graphitization of Co_3Fe_7@NCNTFs and Co_3Fe_7@C. A widely applied method to evaluate the degree of graphitization is to use the intensity ratio of D band to G band, namely I_D/I_G.[21] As shown in **Figure 3b**, the D-band and G-band in our samples are at approximately 1350 cm^{-1} and 1580 cm^{-1}, respectively. The I_D/I_G ratio of Co_3Fe_7@C is 1.45 but decreases

to 0.98 for Co_3Fe_7@NCNTFs, indicating the higher graphitization degree for Co_3Fe_7@NCNTFs, owing to the thermally induced metal catalyzed formation of CNTs.[22]

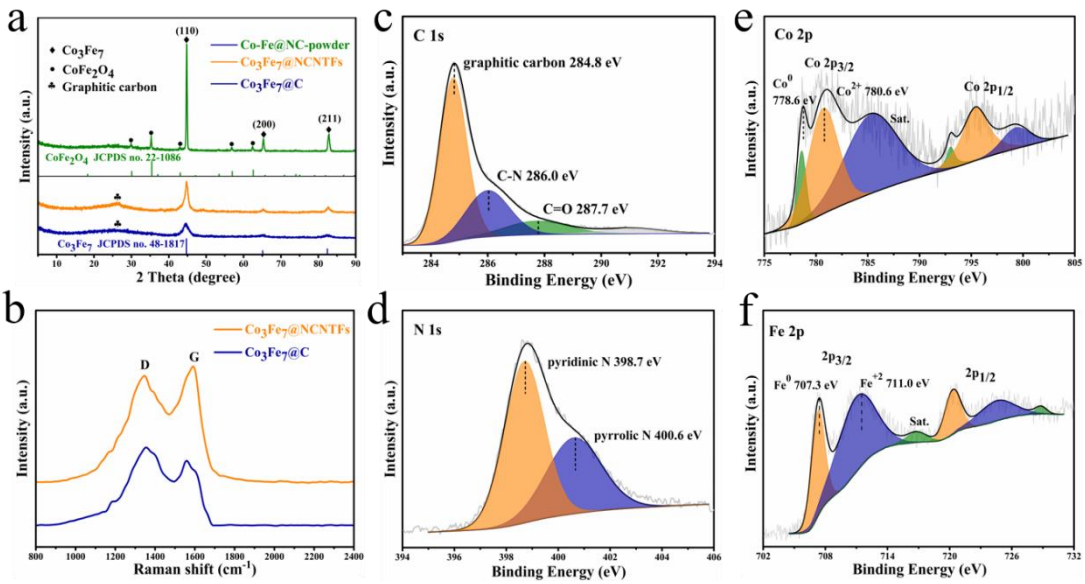

Figure 3. (a) XRD patterns of as-pyrolyzed catalysts and the comparison with Co_3Fe_7 (orange vertical line, JCPDS no. 48-1817) and $CoFe_2O_4$ (green vertical line, JCPDS no. 22-1086); **(b)**, Raman spectra of Co_3Fe_7@NCNTFs and Co_3Fe_7@C. High-resolution XPS spectra of C 1s, N 1s, Fe 2p and Co 2p, respectively; in **(c)**, the fitted peaks correspond to graphitic carbon (284.8 eV), C-N (286.0 eV) and C=O (287.7 eV); **(d)**, the fitted peaks correspond to pyridinic N (398.7 eV) and graphitic N (400.6 eV); **(e)** Co^0 (778.6 eV) and Co^{2+} (780.6 eV). **(f)**, the fitted peaks correspond to Fe^0 (707.3 eV) and Fe^{2+} (711.0 eV).

X-ray photoelectron spectroscopy (XPS) measurements were conducted to investigate the valence state of the bimetallic particles and elucidate the influence of N doping. The survey scan on Co_3Fe_7@NCNTFs reveals the existence of C, N, O, Fe, Co elements (**Figure S5**), the atomic percentages of these elements can be seen in **Table S1**. The deconvolution of the high-resolution C 1s spectrum shows three peaks, which can be assigned to graphitic carbon at ~284.8 eV, C-N at ~286.0 eV, and the C=O at ~287.7 eV (**Figure 3c**).[23] According to the XPS analysis, the atomic percentage of N element in Co_3Fe_7@NCNTFs powder is up to 9.69%, confirming the successful N doping. The high-resolution N 1s spectrum can be deconvolved into two peaks, corresponding to pyridinic N at ~398.7 eV and graphitic N at ~400.6 eV (**Figure 3d**).[24] In addition, the content of pyridinic N is up to ~67%. Previous studies have pointed out that pyridinic nitrogen (N atom is located at the edge of an atomic vacancy) doped in nanotube walls can increase the structural defects of CNTs.[25] These structural imperfections in CNTs are believed to form the adsorption sites for reactants during electrocatalysis.[26] For the Co 2p spectrum, the existence of Co (0) at 778.6 eV of Co $2p_{3/2}$ and Co (II) at 780.6 eV of Co $2p_{3/2}$ are also confirmed (**Figure 3f**).[27] In the Fe 2p spectrum (**Figure 3e**), the two Fe $2p_{3/2}$ peaks located at 707.3 eV and 711.0 eV can be assigned to the Fe (0) and Fe (II) in Co_3Fe_7 nanoparticles, respectively. [27-28]

3.2. Electrochemical Oxygen Evolution and Hydrogen Evolution Activity. According to the above materials characterization analysis, the resulting Co_3Fe_7@NCNTFs demonstrates a unique framework structure composed of interconnected N-doped carbon nanotubes with numerous highly dispersed Co_3Fe_7 nanoparticles, which has the potential to be a promising candidate for water splitting. Firstly, the OER electrocatalytic activity of as-prepared Co_3Fe_7@NCNTFs and control samples were evaluated in 1.0 M KOH alkaline solution using the typical three-electrode device. As shown by the *iR*-corrected polarization curves (**Figure 4a**), the Co_3Fe_7@NCNTFs has the lowest overpotential of 264 mV at 10 mA/cm^2, which is much lower than those of Co-Fe@NC-powder (412 mV) and Co_3Fe_7@C (345 mV). This performance is almost comparable to the commercial RuO_2 electrocatalyst (252 mV at 10 mA/cm^2) and most reported bifunctional electrocatalysts (**Table S2**). The relevant Tafel slopes of all three samples were investigated to analyze the kinetics of the proposed OER reactions (**Figure 4b)**. The Co_3Fe_7@NCNTFs exhibits the lowest Tafel slope of 79 mV/dec, while Co_3Fe_7@C and Co-Fe@NC-powder shows a Tafel slope of 93 mV/dec and 186 mV/dec, respectively. This indicates that Co_3Fe_7@NCNTFs has the favorable rapid reaction kinetics for the OER process, which was further supported by the electrochemical impedance spectroscopy (EIS) shown in **Figure 4c**. Typical EIS consists of the Nyquist plots (spots) and corresponding fitted curves (solid) through applying the inset equivalent circuit. The R_s, R_{ct} and CPE in the equivalent circuit represent the overall ohmic resistance, the charge transfer resistance and the constant phase element, respectively.[29] The fitted results (**Table S3**) reveal that the R_s of Co_3Fe_7@NCNTFs is only 1.5 Ω·cm^2, which is much lower than that of Co_3Fe_7@C (8.6 Ω·cm^2) and Co-Fe@NC-powder (10.9 Ω·cm^2), showing the rather low overall ohmic resistance of Co_3Fe_7@NCNTFs. It is widely accepted that the R_{ct} is correlated to the electrocatalytic kinetics, which means that a smaller R_{ct} indicates a faster reaction rate.[30] From the fitted EIS results, the R_{ct} of Co_3Fe_7@NCNTFs (14.3 Ω·cm^2) is negligible, compared to that of Co_3Fe_7@C (102.5 Ω·cm^2) and Co-Fe@NC-powder (137.2 Ω·cm^2). The smallest charge transfer resistance suggests that the interlaced CNT network structure can significantly enhance the OER reaction kinetics of Co_3Fe_7@NCNTFs.

As a potential candidate to be a bifunctional catalyst, Co_3Fe_7@NCNTFs was further investigated for catalytic HER performance in the identical alkaline environment and electrode configuration employed to OER. As shown in **Figure 4d**, Co_3Fe_7@NCNTFs also shows good HER activity with an overpotential of 197 mV at the current density of 10 mA/cm^2, much lower than that of Co_3Fe_7@C (308 mV) and Co-Fe@NC-powder (372 mV). The promising HER activity of Co_3Fe_7@NCNTFs was further demonstrated by the low Tafel slope. In **Figure 4e,** the Co_3Fe_7@NCNTFs catalyst exhibits the lowest Tafel slope of 62

mV/dec, implying faster reaction kinetics during the electrocatalytic process. It is widely believed that the predominant HER mechanism can be decided by the value of Tafel slope. In alkaline condition, the HER mechanism could be either Volmer-Tafel mechanism or Volmer-Heyrovsky mechanism. The Tafel slope of as-obtained Co_3Fe_7@NCNTFs suggests the favorable HER kinetics following the Volmer-Heyrovsky mechanism[30]

$$H_2O(l)+e^-+*\square \quad H*+OH^-(aq) \quad \text{Volmer reaction (1)}$$

$$H*+H_2O(l)+e^-\square \quad H_2(g)+OH^-(aq)+* \quad \text{Heyrovsky reaction (2)}$$

where, * and H* represent the catalytic sites and absorbed H-species, respectively. The favorable electrocatalytic kinetics of Co_3Fe_7@NCNTFs can also be illustrated by the EIS results (**Figure 4f**). According to the fitted results (**Table S4**), Co_3Fe_7@NCNTFs exhibits significantly small R_{ct} value (23.1 $\Omega\cdot cm^2$), indicating rapid electron transfer process during HER process. The chronoamperometric measurement indicates that both OER and HER exhibit high stability with current retention of 89% and 96%, respectively after being tested for 15 hours (**Figure S6**).

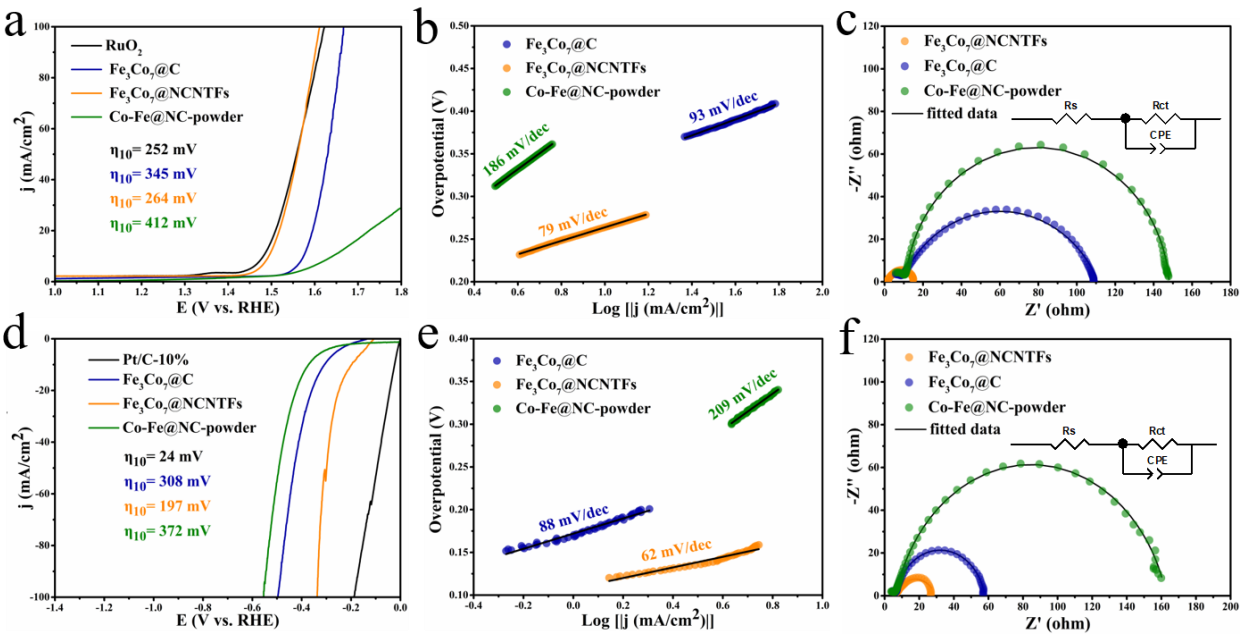

Figure 4. OER electrochemical test. **(a)** OER polarization curves of samples in 1 M KOH solution at a scan rate of 2 mV/s; **(b)** OER Tafel slope plots of samples; **(c)** EIS spectra of corresponding catalysts. (symbols, experimental data; solid lines, fitted results; inset, equivalent circuit). And HER electrochemical test. **(d)** HER polarization curves of samples in 1 M KOH solution at a scan rate of 2 mV/s; **(e)** HER Tafel slope plots of samples; **(f)** EIS spectra of corresponding catalysts. (symbols, experimental data; solid lines, fitted results; inset, equivalent circuit).

3.4. Overall Water Splitting Activity. According to the combined analyses discussed above, the as-obtained Co_3Fe_7@NCNTFs is electrocatalytically active for both OER and HER in alkaline media. Therefore, the overall water splitting activity of the catalyst was studied using Co_3Fe_7@NCNTFs coated

nickel foam as both cathode and anode (**Figure 5a, Figure S7**). In a typical process, at the cathode, Co_3Fe_7 nanoparticles are the main active sites for the HER, where the absorbed H_2O was reduced to H_2 molecules. Similarly, at the anode, the oxygen molecules were also obtained by oxidizing the absorbed OH^-. For comparison, the water electrocatalysis test was also conducted on bare Ni foam electrodes (NF || NF) and Pt/C||RuO_2 electrodes (Pt/C powder coated on nickel foam as cathode, RuO_2 coated on nickel foam as anode).[16] **Figure 5b** shows that a potential of 1.64 V using Co_3Fe_7@NCNTFs is needed to reach a current density of 10 mA/cm^2, which is slightly higher than Pt/C||RuO_2 electrode (1.61 V). In a sharp contrast, to achieve a current density of 10 mA/cm^2, the NF || NF electrode needs to have a high potential of 1.97 V applied to it, which implies that as a substrate, its effect on tested powder catalysts is negligible. The stability/durability of overall water splitting was also evaluated at a potential of 1.64 V (**Figure 5c**). It suggests that the fabricated Co_3Fe_7@NCNTFs, as the bifunctional catalyst, maintains a significantly high electrocatalytic activity after 10 h. The remarkable electrocatalytic performance and high durability of our Co_3Fe_7@NCNTFs powder catalyst are comparable to many state-of-the-art bifunctional electrocatalysts (**Table S2**).

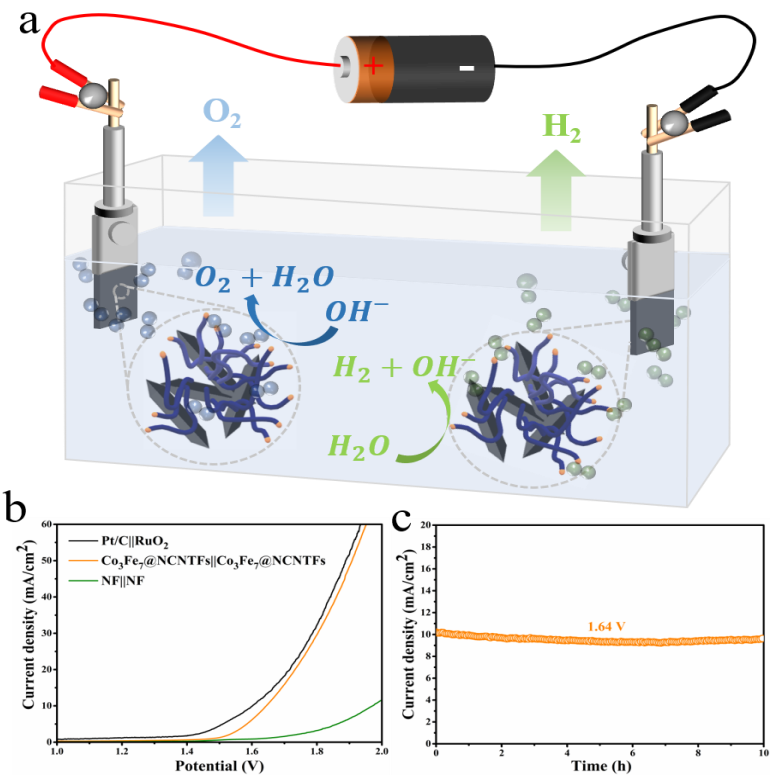

Figure 5. (a) Schematic diagram of the two-electrode configuration for overall water splitting; **(b)** LSV polarization curve of Co-NCNFTs//NF working as both cathode and anode electrode in a 1 M KOH solution for overall water splitting at a scan rate of 2 mV/s; **(c)** Durability test at 1.64 V.

3.5. Mechanistic study on electrocatalyst activity. The chemical composition and the unique

structure of N-doped carbon nanotube frameworks are believed to contribute to the exceptional electrocatalytic activity for both HER and OER. The Co_3Fe_7 nanoparticles embedded in the top of NCNTs play a key role in enhanced electrocatalytic performance for both HER and OER. The highly dispersed and concentrated Co_3Fe_7 nanoparticles, protected and encapsulated by NCNTs, provide a high density of active sites for the studied electrochemical reactions. In addition, the N-doped CNTs also partly contributed to the OER and HER activity. In this work, the content of nitrogen is up to 9.69%, which is significantly higher than most N-doped nanocarbon electrocatalysts.[5a, 16] As mentioned previously, previous studies have confirmed that introducing N atoms can produce structural defects in CNTs and these structural imperfections have been verified being absorption sites for reactant during electrocatalytic process.[26b, 31] In addition, through inducing electronic interactions with neighboring carbon/metal atoms**,** N doping can also provide active sites for electrocatalytic process. Furthermore, the unique porous and interconnected structure of NCNT frameworks facilitates the mass transport during electrocatalytic process without sacrificing electronic conductivity, owing to the high surface area derived from the MOF precursor.[32] The robust three-dimensional (3D) framework, and protective graphitic shell surrounding the Co_3Fe_7 nanoparticles, also endows the electrocatalyst high stability even after working for a long period.

4. CONCLUSIONS

In summary, we have synthesized a high-efficiency bifunctional bimetallic electrocatalyst for overall water splitting (264 mV and 197 mV overpotentials at 10mA/cm^2 current density for OER and HER, respectively) based on the unique micro and nanostructure of our MOF-derived catalysts. The novel hybrid structure of Co_3Fe_7@NCNTFs was produced by employing MIL-88-Fe/Co as starting material and pyrolyzing it with DCDA. During the annealing synthesis, the MIL-88-Fe/Co particles not only provide C source for growth of CNTs catalyzed by the in-situ-reduced metallic Co_3Fe_7 nanoparticles but work as template for formation of nanocarbon frameworks. The resultant Co_3Fe_7@NCNTFs electrocatalyst displays efficient HER and OER electrocatalytic activity with high durability, and outperforms most existing nanocarbon-based catalysts due to the chemical compositions, remarkable conductivity, and robust 3D framework structure. This facile strategy for synthesizing hybrid nanostructure can be employed to develop many other MOF-derived nanocarbon materials and offers a new route for the design of highly efficient and robust electrocatalysts for various electrochemical energy devices.

Conflicts of Interest

There are no conflicts of interest to declare.

Acknowledgement

The Authors are grateful for the financial support from the National Natural Science Foundation of China (grant nos. 51201004 and 61671040) and the Australian Research Council (CE140100012). The Authors would like to thank the Australian National Fabrication Facility (ANFF) – Materials Node, UOW.

Reference

[1] D. Kong, J. J. Cha, H. Wang, H. R. Lee, Y. Cui, *Energy Environ. Sci.* **2013**, *6*, 3553.

[2] T. E. Mallouk, *Nat. Chem.* **2013**, *5*, 362-363.

[3] a) X. Zhang, X. Zhang, H. Xu, Z. Wu, H. Wang, Y. Liang, *Adv. Funct. Mater.* **2017**, *27*, 1606635; b) M. Wang, Y. Li, C. Feng, G. Zhao, Z. S. Wang, *Chem.-Asian J.* **2019**, *14*, 1034-1041.

[4] a) Y. Yan, B. Y. Xia, B. Zhao, X. Wang, *J. Mater. Chem. A* **2016**, *4*, 17587-17603; b) H. Jin, J. Wang, D. Su, Z. Wei, Z. Pang, Y. Wang, *J. Am. Chem. Soc.* ***2015****, 137, 2688-2694.*

[5] a) B. Y. Xia, Y. Yan, N. Li, H. B. Wu, X. W. Lou, X. Wang, *Nat. Energy* **2016**, *1*; b) H. Wang, H.-W. Lee, Y. Deng, Z. Lu, P.-C. Hsu, Y. Liu, D. Lin, Y. Cui, *Nat. Commun.* **2015**, *6*.

[6] a) Y. Wang, T. Zhou, K. Jiang, P. Da, Z. Peng, J. Tang, B. Kong, W.-B. Cai, Z. Yang, G. Zheng, *Adv. Energy Mater.* **2014**, *4*, 1400696; b) H. Hu, B. Guan, B. Xia, X. W. Lou, *J. Am. Chem. Soc.* **2015**, *137*, 5590-5595.

[7] H. Fang, T. Huang, Y. Sun, B. Kang, D. Liang, S. Yao, J. Yu, M. M. Dinesh, S. Wu, J. Y. Lee, S. Mao, *J. Catal.* **2019**, *371*, 185-195.

[8] Y. Guo, T. Park, J. W. Yi, J. Henzie, J. Kim, Z. Wang, B. Jiang, Y. Bando, Y. Sugahara, J. Tang, Y. Yamauchi, *Adv. Mater.* **2019**, *31*, 1807134.

[9] N. Coleman, M. D. Lovander, J. Leddy, E. G. Gillan, *Inorg. Chem.* **2019**, *58*, 5013-5024.

[10] E. L. K. Chng, M. Pumera, *Chem.-Asian J.* **2011**, *6*, 2304-2307.

[11] D. Ding, K. Shen, X. Chen, H. Chen, J. Chen, T. Fan, R. Wu, Y. Li, *ACS Catal.* **2018**, *8*, 7879-7888.

[12] a) Y. Zhou, H. Xue, T. Wang, H. Guo, X. Fan, L. Song, W. Xia, H. Gong, Y. He, J. Wang, J. He, *Chem.-Asian J.* **2017**, *12*, 60-66; b) X. Han, W. Zhang, X. Ma, C. Zhong, N. Zhao, W. Hu, Y. Deng, *Adv. Mater.* **2019**, *31*, 1808281.

[13] M. Zhang, Q. Dai, H. Zheng, M. Chen, L. Dai, *Adv. mater.* **2018**, *30*, 1705431; b) S.-K. Park, Y. C. Kang, *ACS Appl. Mater. Interfaces* **2018**, *10*, 17203-17213.

[14] Y. Deng, B. Chi, J. Li, G. Wang, L. Zheng, X. Shi, Z. Cui, L. Du, S. Liao, K. Zang, J. Luo, Y. Hu, X. Sun, *Adv. Energy Mater.* **2019**, *9*, 1802856.

[15] S.-K. Park, Y. C. Kang, *ACS Appl. Mater. Interfaces* **2018**, *10*, 17203-17213.

[16] X. Zhao, P. Pachfule, S. Li, J. R. J. Simke, J. Schmidt, A. Thomas, *Angew. Chem.-Int. Edit.* **2018**, *57*, 8921-8926.

[17] a) Q. Yuan, Y. Yu, Y. Gong, X. Bi, *ACS Appl. Mater. Interfaces* **2019**, *12*, 3592-3602; b) T. Ouyang, Y.-Q. Ye, C.-Y. Wu, K. Xiao, Z.-Q. Liu, *Angew. Chem.-Int. Edit.* **2019**, *58*, 4923-4928; c) Y. Li, M. Lu, P. He, Y. Wu, J. Wang, D. Chen, H. Xu, J. Gao, J. Yao, *Chem.-Asian J.* **2019**, *14*, 1590-1594.

[18] T. Tang, W. J. Jiang, S. Niu, N. Liu, H. Luo, Y. Y. Chen, S. F. Jin, F. Gao, L. J. Wan, J. S. Hu, *J. Am. Chem. Soc.* **2017**, *139*, 8320-8328.

[19] J. Meng, C. Niu, L. Xu, J. Li, X. Liu, X. Wang, Y. Wu, X. Xu, W. Chen, Q. Li, Z. Zhu, D. Zhao, L. Mai, *J. Am. Chem. Soc.* **2017**, *139*, 8212-8221.

[20] a) S. S. Maklakov, S. A. Maklakov, I. A. Ryzhikov, V. A. Amelichev, K. V. Pokholok, A. N. Lagarkov, *J. Alloy. Compd.* **2012**, *536*, 33-37; b) S. Wang., Z. Deng., J. Li., H. Liu., Y. Wang., X. Fu., *IOP Conf. Ser.: Mater. Sci. Eng*. **2019**, *592*, 012043.

[21] J. Zhou, Y. Dou, A. Zhou, R.-M. Guo, M.-J. Zhao, J.-R. Li, *Adv. Energy Mater.* **2017**, *7*, 1602643.

[22] I. S. Amiinu, Z. Pu, X. Liu, K. A. Owusu, H. G. R. Monestel, F. O. Boakye, H. Zhang, S. Mu, *Adv. Funct. Mater.* **2017**, *27*, 1702300.

[23] a) X. Jian, X. Liu, H.-m. Yang, J.-g. Li, X.-l. Song, H.-y. Dai, Z.-h. Liang, *Appl. Surf. Sci.* **2016**, *370*, 514-521; b) K. Kishi., Y. Okino., Y. Fujimoto., *Surface Science* **1986**, *176*, 23-31.

[24] a) Y. Xie, Y. Chen, L. Liu, P. Tao, M. Fan, N. Xu, X. Shen, C. Yan, *Adv. mater.* **2017**, *29*; b) N. Hellgren, R. T. Haasch, S. Schmidt, L. Hultman, I. Petrov, *Carbon* **2016**, *108*, 242-252.

[25] a) L. G. Bulusheva, A. V. Okotrub, I. A. Kinloch, I. P. Asanov, A. G. Kurenya, A. G. Kudashov, X. Chen, H. Song, *phys. status solidi (b)* **2008**, *245*, 1971-1974; b) S. H. Lim, H. I. Elim, X. Y. Gao, A. T. S. Wee, W. Ji, J. Y. Lee, J. Lin, *Phys. Rev. B* **2006**, *73*.

[26] a) H. T. Chung, J. H. Won, P. Zelenay, *Nat. Commun.* **2013**, *4*; b) F. Jaouen, A. M. Serventi, M. LefŁvre, J. P. Dodelet, P. Bertrand, *J. Phys. Chem. C* **2007**, *111*, 5971-5976.

[27] X. Yuan, X. Wang, M. S. Riaz, C. Dong, Z. Zhang, F. Huang, *Catal. Sci. Technol.* **2018**, *8*, 2427-2433.

[28] C. Pirlot., J. Delhalle., J. J. Pireaux., Z. Mekhalif., *Surf. Coat. Tech.* **2001**, *138*, 166-172.

[29] a) G.-F. Chen, T. Y. Ma, Z.-Q. Liu, N. Li, Y.-Z. Su, K. Davey, S.-Z. Qiao, *Adv. Funct. Mater.* **2016**, *26*, 3314-3323; b) X. Cui, B. Zhang, C. Zeng, H. Wen, S. Guo, *Int. J. Hydrog. Energy* **2018**, *43*, 15234-15244.

[30] H. Zhang, X. Li, A. Hähnel, V. Naumann, C. Lin, S. Azimi, S. L. Schweizer, A. W. Maijenburg, R. B. Wehrspohn, *Adv. Funct. Mater.* **2018**, *28*, 1706847.

[31] H. Jiang, J. Gu, X. Zheng, M. Liu, X. Qiu, L. Wang, W. Li, Z. Chen, X. Ji, J. Li, *Energy Environ. Sci.* **2019**, *12*, 322-333.

[32] a) W. Chaikittisilp, K. Ariga, Y. Yamauchi, *J. Mater. Chem. A* **2013**, *1*, 14-19; b) S. Lim, K. Suh, Y. Kim, M. Yoon, H. Park, D. N. Dybtsev, K. Kim, *Chem. Commun.* **2012**, *48*, 7447.